Crossover from tricritical to critical end point behavior in free-standing smectic films

Maria S. S. Pereira, Italo N. de Oliveira, and Marcelo L. Lyra*
Instituto de Física, Universidade Federal de Alagoas, 57072-970 Maceió, Alagoas, Brazil
(Received 21 September 2011; published 28 December 2011)

We study the smectic to nematic (SmA-N) phase transition taking place at the center of a free-standing film that exhibits enhanced surface order due to the anchoring promoted by a surrounding gas. The usual McMillan mean-field approach predicts that the SmA-N transition in bulk samples can be continuous or discontinuous (first or second order) depending on the molecular geometry, with a tricritical point separating these two regimes. Here we show that the additional orientational order imposed by the surface anchoring stabilizes the surface-induced smectic and nematic phases, leading to the breakdown of the tricritical point and to the emergence of a critical end point. We report the full phase diagram, which depicts four distinct structures as the film thickness is reduced.

DOI: 10.1103/PhysRevE.84.061706 PACS number(s): 61.30.Hn, 64.70.mf, 68.35.Md

I. INTRODUCTION

Surface effects are particularly important in the study of phase transitions in liquid crystals. Due to the strong anchoring of the molecules at the interface, the order near the surface is usually stronger than in the bulk. Surface-phase transitions in liquid crystals show a diverse phenomenology, such as the emergence of a surface-induced smectic phase [1–4], layer-by-layer thinning [5], and an anomalous nonmonotonic thickness dependence of the transition temperature [6,7]. The interplay between field and surface effects has also been explored in the literature. In particular, it has been shown that an external electric field can induce layer thinning transitions in compounds with negative dielectric anisotropy [8], while it stabilizes a parasmectic surface phase in compounds with a positive dielectric anisotropy [2]. A magnetic-field-induced order in a thermotropic liquid crystal has also been experimentally demonstrated [9]. The similarity and dissimilarity between the influences of anchoring walls and external fields on nematic and smectic phases has been recently discussed [1].

Free-standing smectic films provide an ideal experimental setup to study surface-induced ordering effects [5–8,10–14]. In these films, the enhanced order near the surfaces is due to the surface tension between the film and the surrounding gas, which controls the nature of a long-ranged fluctuation-induced force between the film surfaces [15,16]. It has been recently reported, for example, that the critical exponent of the biaxiality is smaller for the surface transition than for the interior transition [12], corroborating the theoretical prediction of a lower dimensionality of the surface critical behavior. In addition, a helical smectic phase has been shown to disappear in a chiral antiferroelectric free-standing thin film as a result of the joint effects of reduced dimensionality and surface ordering [17]. However, a complete understanding of the influence of surface ordering on the phase transition taking place in the interior of free-standing thin films is still lacking.

A discrete version of the McMillan model including the surface anchoring at the liquid crystal-gas interface has been able to reproduce qualitatively as well as quantitatively many features related to the layer thinning transitions of smectic liquid crystal films [18–20]. Here we will show that, within such a mean-field approach, the phase diagram associated with the transitions at the film center displays dramatic changes as the film thickness is reduced. While four phases (smectic, nematic, and surface-induced smectic and nematic) can be attained at thick films, only two of them (smectic and surface-induced nematic) remain stable in thin films. Further, the tricritical point of bulk samples splits into a critical point and a more uncommon critical end point. Critical end point behavior has been shown to appear in other physical scenarios such as fluid mixtures [21], wetting phenomena [22], disordered systems [23], magnetic materials [24], metals [25], superconductors [26], and quantum chromodynamics [27]. Free-standing smectic films then appear as a new experimental setup to probe the critical end point behavior.

II. DISCRETE MCMILLAN MEAN-FIELD MODEL

The inhomogeneity of the nematic and smectic order parameter profiles in thin smectic films can be properly accounted for by the discrete extension of the McMillan mean-field model [18–20]. In this approach, the system can be described by a stack of N two-dimensional layers with normal along the z axis. The layer thickness is taken to be of the same order of the smectic layer thickness d. Therefore each layer has its own nematic s_n and smectic σ_n order parameters. The effective one-body potential felt by a molecule in an interior layer located at z_i and oriented with an azimuthal angle θ_i can be written as [19]

$$V_i(z_i,\theta_i) = -V_0\,[\bar{s}_i + \alpha\bar{\sigma}_i\cos(2\pi z_i/d)]\,P_2(\cos\theta_i)\,, \qquad (1)$$

where V_0 is a typical interaction energy that determines the scale of the nematic-isotropic transition temperature in bulk samples and α is a geometric parameter related to the ratio between the rigid length r_0 of calamitic molecules and the layer thickness d. In fact, the values for the α parameter can be directly associated with the length of alkyl tails in different compounds of a homologous series. $P_2(\cos\theta_i)$ is the second-order Legendre polynomial. In this approach, the local one-body potential is given in terms of the average nematic $\bar{s}_i$ and smectic $\bar{\sigma}_i$ order parameters on the ith layer and its two neighboring layers. At each surface layer, the anchoring and the missing volume effects are effectively taken into account by a homeotropic surface orientational field of strength W_0 [19,28]. The effective one-body potential at the top surface

*marcelo@fis.ufal.br

layer retains the general form of Eq. (1) but with the order parameter averages replaced by $\bar{s_1} = (s_1 + s_2 + 3W_0/V_0)/3$ and $\bar{\sigma_1} = (\sigma_1 + \sigma_2)/3$, with similar equations holding at the bottom layer. It has been shown that the above model reproduces quantitatively well the layer thinning transitions [20] that take place for $W_0 > V_0/4$. In what follows, we will consider a strong anchoring $W_0/V_0 = 3$, at which the surface ordering effects are prominent. At the end of next section, we provide a discussion on the influence of the relative surface anchoring strength on the phase diagram.

The local order parameters s_i and σ_i satisfy the set of self-consistent equations $s_i = \langle P_2(\cos\theta_i)\rangle_i$ and $\sigma_i = \langle P_2(\cos\theta_i)\cos(2\pi z_i/d)\rangle_i$ $(i = 1,2,\ldots N)$. Thermodynamic averages are computed from the one particle distribution function in the ith smectic layer $f_i(z_i,\theta_i) \propto \exp[-V_i/k_BT]$. In the cases for which the self-consistent equations provide multiple solutions for the order parameter profiles (near first-order transitions), the thermodynamically stable solution corresponds to the global minimum of the Helmholtz free energy [20,29]. This model predicts a similar McMillan's phase diagram at the central layer when the film thickness is much larger than the surface penetration length [30]. However, a distinct scenario takes place at the center of thin films due to the strong influence of surface ordering, as we detail below.

III. LIQUID-CRYSTALLINE ORDER IN THIN FILMS

We start by reporting the temperature dependence of the nematic (Fig. 1) and smectic (Fig. 2) order parameters at the central layer for a series of values of the geometrical parameter α and four representative film thicknesses, $N = 5,9,15$, and 41. For the thicker film [$N = 41$, Figs. 1(a) and 2(a)], the sequence of transitions is similar to the one predicted by the McMillan theory for bulk samples. At small values of

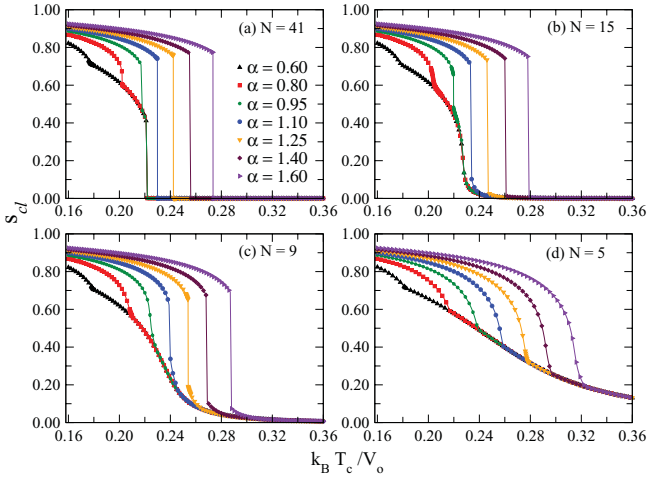

FIG. 1. (Color online) Temperature dependence of the nematic order parameter at the central layer for several values of the geometric parameter α and four representative film thicknesses: (a) $N = 41$, (b) $N = 15$, (c) $N = 9$, and (d) $N = 5$. In each plot, the geometric parameter α increases from the left ($\alpha = 0.6$) to the right ($\alpha = 1.6$). For very thin films there is no discontinuity of the nematic order irrespective of the value of α. Two discontinuous transitions set up at some specific range of α values for thick films. The surface-induced nematic order at the central layer vanishes as $N \to \infty$.

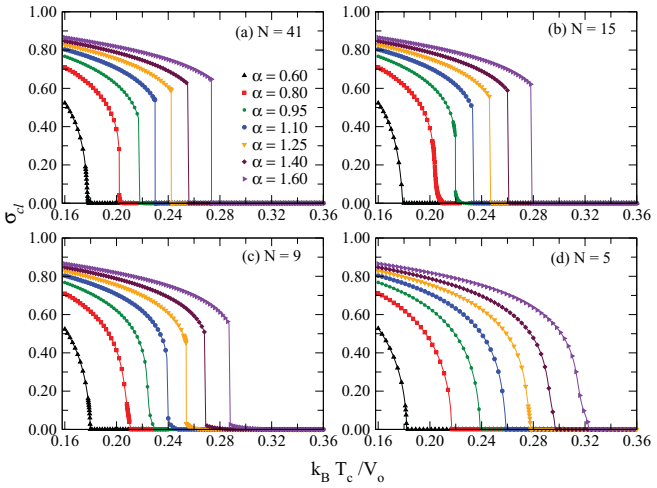

FIG. 2. (Color online) Temperature dependence of the smectic order parameter at the central layer for several values of the geometric parameter α and four representative film thicknesses: (a) $N = 41$, (b) $N = 15$, (c) $N = 9$, and (d) $N = 5$. In each plot, the geometric parameter α increases from the left ($\alpha = 0.6$) to the right ($\alpha = 1.6$). For very thin films there is only a continuous transition where the smectic order vanishes continuously. At larger thicknesses, there appears a jump on the smectic order to a small finite value (surface-induced smectic order) for a range of α values. For large α the smectic order jumps directly to zero. The surface-induced smectic phase shrinks as N increases.

α the smectic order parameter decays continuously, while the nematic order remains finite, a signature of the second-order smectic-nematic transition. At a higher temperature, the nematic order displays a discontinuity at the nematic-isotropic first-order transition. In practice, the transition to the nematic phase leads to the film thinning or to the film rupture. As α increases, the smectic order parameter develops a discontinuity at the transition, resulting also in a jump on the nematic order to a smaller finite value (first-order smectic-nematic transition) prior to the ultimate nematic-isotropic transition. At large values of α, only a direct first-order smectic-isotropic transition is observed.

In the vicinity of the crossover from the first- to second-order smectic-nematic transition, the smectic order parameter rounds, pointing out to a residual smectic order. This region is better identified at thinner films. In Figs. 1(b) and 2(b) we show the nematic and smectic order parameters at the center of a film with $N = 15$ layers. The rounding of the smectic order parameter is quite evident at $\alpha = 0.80$ and 0.95. In the first case, the transition is still continuous, differing from the discontinuous transition predicted by McMillan's theory for bulk samples. However, a residual smectic order parameter persists after the jump in the latter case. Further, the nematic order vanishes smoothly as the temperature is raised, signaling the absence of the nematic-isotropic transition. The strong surface anchoring is responsible for such residual order at the film center. A residual nematic order shall persist even at thicker films, but it is too small at the film center to be noticed at the scale shown. Therefore the isotropic phase is actually replaced by a surface-induced nematic phase (si-N). Similarly,

the nematic phase with a residual smectic order can be termed a surface-induced smectic phase (si-SmA).

In Figs. 1(c) and 2(c) the order parameters at the center of a film with $N = 9$ layers are shown. In this case, there is no direct discontinuous transition from the smectic to the surface-induced nematic phase. There is always an intermediate surface-induced smectic phase. The direct transition is always second order, taking place at small values of α. Finally, at very thin films (see Figs. 1(d) and 2(d) for a film with $N = 5$ layers), only a single continuous transition from the smectic to the surface-induced nematic phase persists.

The trends discussed above can be summarized in four distinct structures for the phase diagram, as shown in Fig. 3. For thick films, the phase diagram is quite similar to that depicted by bulk samples. However, there is a very prominent change concerning the tricritical point that delimits the second- and first-order smectic-nematic transitions in bulk samples. In particular, the tricritical point splits into a critical point and a critical end point. In this case, the critical point corresponds to the end of the coexistence line between the smectic and surface-induced smectic. On the other hand, the critical end point represents the position at which the line of continuous transitions between the surface-induced smectic and surface-induced nematic phases encounters the coexistence lines between the smectic and the nematic and surface-induced smectic phases. The critical end point moves toward the triple point (the coexistence of the smectic, nematic, and surface-induced nematic phases). When it reaches the triple point, the discontinuous transition between the nematic and surface-induced nematic disappears, as shown in Fig. 3(b) for $N = 15$. In this case, the nematic order smoothly decays with increasing temperatures. At thinner films, the second- and first-order transition lines do not meet each other [see Fig. 3(c)]. The phase-diagram has a single critical point at the end of the coexistence line between the smectic and surface-induced smectic phases. For very thin films, only the smectic to surface-induced nematic continuous transition persists, as represented in Fig. 3(d) for $N = 5$ layers.

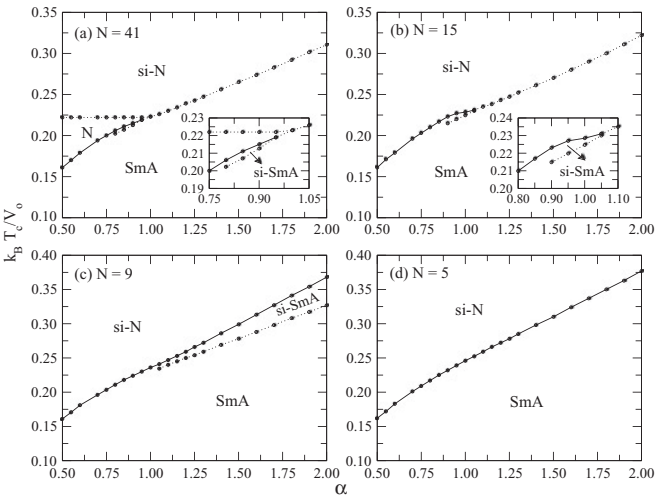

FIG. 3. The phase diagram in the T vs α parameter space for representative film thicknesses: (a) $N = 41$, (b) $N = 15$, (c) $N = 9$, and (d) $N = 5$. Solid (dotted) lines correspond to second-order (first-order) transitions. For thick films, the phase diagram is similar to the one of bulk systems. However, the isotropic phase is replaced by a surface-induced nematic phase, and the tricritical point splits into a critical point and a critical end point. A small surface-induced smectic phase appears (see insets). As the film thickness decreases, the discontinuous transition between the nematic and surface-induced nematic phase disappears, followed by the disappearance of the critical end point. A single continuous transition between the smectic and the surface-induced nematic phases remains for very thin films.

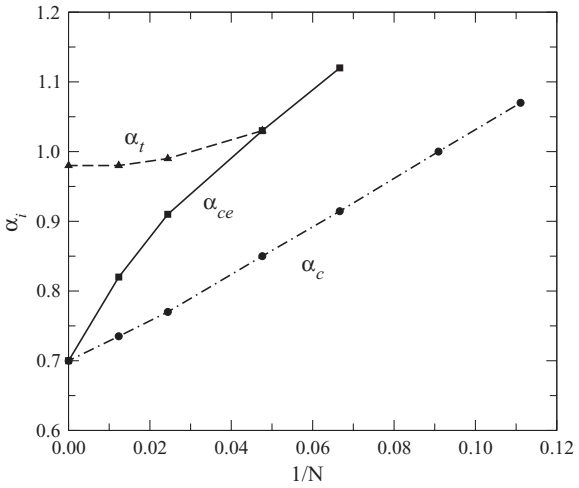

FIG. 4. Thickness dependence of the value of the geometric parameter α at the triple point α_t, at the critical end point α_{ce}, and at the critical point α_c. As $1/N \to 0$, α_c and α_{ce} merge at the bulk tricritical point. For $N < 20$ the triple point disappears with the nematic phase [see Fig. 3(b)] . For $N < 15$ the critical end point disappears because the first- and second-order transition lines split [see Fig. 3(c)]. There is no critical point for $N < 9$ as the transition between the smectic and surface-induced nematic phases becomes always continuous.

Therefore, the phase diagram of free-standing smectic films may display up to three special points: a triple point, a critical point, and a critical end point. The last two merge in a tricritical point as the film thickness increases. On the other hand, all of them disappear in the limit of very thin films because surface orientational ordering plays a predominant role. The thickness dependence of the value of the geometric factor α for each special point is shown in Fig. 4. For thick films the phase diagram has all three special points once all four possible phases can be reached, namely, smectic, surface-induced smectic, nematic, and surface-induced nematic. There is a first intermediate regime, for $15 < N < 20$, in which the triple point is absent. In a second intermediate regime, with thickness ranging from $9 < N < 15$, the critical end point also disappears. In these intermediate thickness regimes, only three phases are stable: smectic, surface-induced smectic, and surface-induced nematic. At the end, the phase diagram has no special point for $N < 9$ and only two phases (smectic and surface-induced nematic) persist.

The exact range of thicknesses for each regime depends on the strength of the surface anchoring. In particular, the characteristic penetration length of the surface-induced order becomes smaller when the ratio between the anchoring energy and the typical intermolecular interaction potential decreases. Therefore, some features of the phase diagram are shifted

toward thinner films such as the coalescence of the triple and critical end points, the ultimate disappearance of the critical end point, and the total fade off of the surface-induced smectic phase. Actually, within the present discrete mean-field approach, surface enhancement only surpasses finite-size effects when the anchoring energy is above a characteristic value [8,20]. In fact, surface-induced effects are continuously reduced when the surface energy decreases. In this way, the last stages of the phase diagram, here reported to hold for strongly anchored thin films, may not be reachable at weak surface energies. A detailed study of the anchoring strength influence on the phase diagram is out of the main focus of the present work, which is to reveal the breakdown of the tricritical point and the emergence of a critical end point. A complete analysis of the dependence of the phase diagram on the anchoring energy will be presented in a future contribution.

We would like to call attention to the fact that strongly anchored free-standing smectic films usually depict layer thinning transitions as the temperature is raised [5]. The melting of the smectic order at the central layer is followed by the expulsion of the melted material to the meniscus, resulting in a thinner smectic film. Therefore, the transitions from the smectic to the nematic phases may only be probed when approaching the transition from low temperatures. As a final remark, the residual order in the surface-induced smectic phase is usually small, which may make its experimental observation difficult because fluctuations may lead to the film rupturing. However, experiments on free-standing films as thin as two layers [31–33] and measurements of anchoring energies strong enough to support surface-enhanced order [28] point toward the feasibility of experimental tests of the predicted phase diagrams.

IV. SUMMARY AND CONCLUSIONS

In summary, we provided a detailed picture of the phase transitions taking place at the interior of free-standing smectic films. Within the scope of a mean-field-like discrete McMillan theory, we showed that the inner layers of free-standing films may exhibit a thickness dependent sequence of phase transitions due to the surface ordering imposed by the anchoring at the interfaces of the film with the surrounding gas. In particular, we reported that the central layer may display a discontinuous transition from the usual smectic to a surface-induced smectic phase, which becomes more prominent in an intermediate regime of film thicknesses. At very thin films, there is only a direct transition between the smectic and a surface-induced nematic phase. Associated with the emergence of such an intermediate surface-induced smectic phase, there appear special points in the phase diagram. The well-known tricritical point separating the continuous from the discontinuous smectic-nematic phase transition in bulk samples splits into a critical point and a critical end point. Therefore, the original discontinuous smectic-nematic bulk transition is strongly affected as the film thickness is reduced. In fact, such a bulk transition splits at a critical end point into a discontinuous smectic to surface-induced smectic transition, followed by a continuous surface-induced smectic to surface-induced nematic transition. Further thinning leads to the disappearance of the surface-induced smectic phase, and a single continuous transition from the smectic to the surface-induced nematic takes place. It is important to stress that the range of the geometric parameter α used to compute the present results is compatible with some homologous series, such as n-cyanobiphenyl (nCB) and N-alkylpyridinium dodecylsulphates (nPySO4m) series [34]. Because experimental techniques to study phase transitions in free-standing smectic films have been well developed over the last decades, the presently proposed scenario suggests this single component physical system as a potential candidate to probe the critical end point behavior without the need of controlling external fields or mixture concentrations.

ACKNOWLEDGMENTS

We would like to thank CAPES, Instituto Nacional de Ciência e Tecnologia de Fluidos Complexos (INCT-FCx), CNPq, and FINEP (Brazilian research agencies) as well as FAPEAL (Alagoas State Research Agency) for partial financial support.

[1] M. Torikai and M. Yamashita, Mol. Cryst. Liq. Cryst. **441**, 59 (2005).
[2] P. Galatola, M. Zelazna, and I. Lelidis, Eur. Phys. J. B **2**, 51 (1998).
[3] I. Lelidis and P. Galatola, Phys. Rev. E **66**, 010701(R) (2002).
[4] D. de las Heras, Y. Martinez-Raton, and E. Velasco, Phys. Rev. E **81**, 021706 (2010).
[5] T. Stoebe, P. Mach, and C. C. Huang, Phys. Rev. Lett. **73**, 1384 (1994).
[6] R. Geer, T. Stoebe, and C. C. Huang, Phys. Rev. B **45**, 13055 (1992).
[7] C. Y. Chao, C. R. Lo, P. J. Wu, T. C. Pan, M. Veum, C. C. Huang, V. Surendranath, and J. T. Ho, Phys. Rev. Lett. **88**, 085507 (2002).
[8] M. S. S. Pereira, M. L. Lyra, and I. N. de Oliveira, Phys. Rev. Lett. **103**, 177801 (2009).
[9] T. Ostapenko, D. B. Wiant, S. N. Sprunt, A. Jákli, and J. T. Gleeson, Phys. Rev. Lett. **101**, 247801 (2008).
[10] R. Pindak, W. O. Sprenger, D. J. Bishop, D. D. Osheroff, and J. W. Goodby, Phys. Rev. Lett. **48**, 173 (1982).
[11] Ch. Bahr, Phys. Rev. Lett. **99**, 057801 (2007).
[12] L. D. Pan, B. K. McCoy, S. Wang, W. Weissflog, and C. C. Huang, Phys. Rev. Lett. **105**, 117802 (2010).
[13] T. Stoebe, R. Geer, C. C. Huang, and J. W. Goodby, Phys. Rev. Lett. **69**, 2090 (1992).
[14] Ch. Bahr and D. Fliegner, Phys. Rev. Lett. **70**, 1842 (1993).
[15] L. V. Mikheev, Zh. Eksp. Teor. Fiz. **96**, 632 (1989) [Sov. Phys. JETP **69**, 358 (1989)].
[16] I. N. de Oliveira and M. L. Lyra, Phys. Rev. E **65**, 051711 (2002); **70**, 050702(R) (2004).
[17] L. D. Pan, S. Wang, C. S. Hsu, and C. C. Huang, Phys. Rev. Lett. **103**, 187802 (2009).

[18] W. L. McMillan, Phys. Rev. A **4**, 1238 (1971).
[19] L. V. Mirantsev, Phys. Lett. A **205**, 412 (1995).
[20] A. A. Canabarro, I. N. de Oliveira, and M. L. Lyra, Phys. Rev. E **77**, 011704 (2008).
[21] N. B. Wilding, Phys. Rev. Lett. **78**, 1488 (1997).
[22] S. Rafaï, D. Bonn, E. Bertrand, J. Meunier, V. C. Weiss, and J. O. Indekeu, Phys. Rev. Lett. **92**, 245701 (2004).
[23] A. Falicov and A. N. Berker, Phys. Rev. Lett. **76**, 4380 (1996).
[24] L. Demkó, I. Kézsmárki, G. Mihály, N. Takeshita, Y. Tomioka, and Y. Tokura, Phys. Rev. Lett. **101**, 037206 (2008).
[25] M. Dzero, M. R. Norman, I. Paul, C. Pépin, and J. Schmalian, Phys. Rev. Lett. **97**, 185701 (2006).
[26] J.-P. Rueff, S. Raymond, M. Taguchi, M. Sikora, J.-P. Itié, F. Baudelet, D. Braithwaite, G. Knebel, and D. Jaccard, Phys. Rev. Lett. **106**, 186405 (2011).
[27] S. X. Qin, L. Chang, H. Chen, Y. X. Liu, and C. D. Roberts, Phys. Rev. Lett. **106**, 172301 (2011).
[28] Z. Li and O. D. Lavrentovich, Phys. Rev. Lett. **73**, 280 (1994).
[29] A. V. Zakharov and D. E. Sullivan, Phys. Rev. E **82**, 041704 (2010).
[30] J. V. Selinger and D. R. Nelson, Phys. Rev. A **37**, 1736 (1988).
[31] T. Stoebe, C. C. Huang, and J. W. Goodby, Phys. Rev. Lett. **68**, 2944 (1992).
[32] Ch. Bahr and D. Fliegner, Phys. Rev. Lett. **70**, 1842 (1993).
[33] C. Y. Chao, C. F. Chou, J. T. Ho, S. W. Hui, A. Jin, and C. C. Huang, Phys. Rev. Lett. **77**, 2750 (1996).
[34] S. Urban, J. Przedmojski, and J. Czub, Liq. Cryst. **32**, 619 (2005); C. Cruz, B. Heinrich, A. C. Ribeiro, D. W. Bruce, and D. Gulon, *ibid.* **27**, 1625 (2000).